ARTICLE

Sequential Coating of Magnetic Carbonyliron Particles with Polystyrene and Multiwalled Carbon Nanotubes and Its Effect on Their Magnetorheology

Fei Fei Fang,[†] Hyoung Jin Choi,*[,†] and Yongsok Seo[‡]

Department of Polymer Science and Engineering, Inha University, Incheon 402-751, Korea, and School of Materials Science and Engineering, Seoul National University, Seoul 151-744, Korea

ABSTRACT A two-step process for the sequential coating of magnetic carbonyliron (CI) particles with polystyrene (PS) and multiwalled carbon nanotubes (MWCNTs) was used to improve the sedimentation stability of micrometer-sized magnetic CI particles for magnetorheological (MR) applications under an applied magnetic field. The CI particles were initially coated with nanosized PS beads using an in situ dispersion polymerization method and then wrapped with a dense MWCNT nest through a solvent-casting method in a water/oil emulsion system. The morphology, MR performance, and sedimentation stability of the synthesized magnetic composite particles were examined. The composite particles showed enhanced MR characteristics and dispersion stability.

KEYWORDS: magnetorheological fluid • carbonyliron • polystyrene • multiwalled carbon nanotube • coating

1. INTRODUCTION

Since their discovery, magnetorheological (MR) colloidal suspensions consisting of magnetic particles dispersed in a nonmagnetic medium oil are considered to be one of several intelligent materials. They can be transformed reversibly from a fluidlike state to a solidlike phase within milliseconds under an applied magnetic field, showing drastic changes in their rheological characteristics (1−8). Although their performances are similar to those of electrorheological (ER) fluids under an applied electric field (9−11), MR fluids exhibit a far superior yield behavior under an applied magnetic field and have been considered to be good candidates for potential engineering applications in the design of dampers, brakes, polishing machine, or torque transducers (12, 13).

However, MR fluids still require significant improvement in their suspension stability and control of their colloidal properties. The reasons lie mainly in the intrinsic properties of the dispersed phase of MR fluids, in which magnetic carbonyliron (CI) particles have been widely adopted as a dispersed phase for MR fluids because of their high saturation magnetization and proper particle size (14−17). However, the large density of CI particles, which causes a serious sedimentation problem, has limited their further engineering applications. Therefore, considerable efforts (introducing additives or polymer-coating technology) have been made to prevent CI particles from coming in contact with each other and to decrease the CI particle density to improve the sedimentation stability (18−21). Among them, polymer-coating technology becomes more and more prevailing because of the favorable morphology and significant decrease in the density of the resulting magnetic particle, both of which can contribute to the improved sedimentation characteristics. Hence, there has been considerable effort on coating CI with either polymers (14, 20) or multiwalled carbon nanotubes (MWCNTs). Note that Pu et al. (5) also reported MR fluids based on glycol, iron powder, poly(vinylpyrrolidone) (PVP), and MWCNT, in which the PVP and MWCNT acted as additives to improve the sedimentation stability of the MR fluid.

Embedding CI into polymeric microbeads was also attempted. However, the morphology and thickness of the coated polymeric shell are influenced easily by the mole ratio of reactants, as well as by the grafting agent or reaction temperature selected. In addition, the smooth surface of polymer-coated CI particles might not always have a positive effect on improving the sedimentation problem. Therefore, nanoscaled polystyrene (PS) beads were initially deposited on the surface of CI particles through conventional dispersion polymerization. Subsequently, based on the self-assembling properties of MWCNT (23), densely piled MWCNT nests were constructed over the surface of the PS-coated CI particles by a simple solvent-casting method in a water/oil (W/O) emulsion system, in which the MWCNTs were introduced to the MR fluids for better dispersion (22). The surface morphology was examined in stages. The MR performances based on the synthesized MWCNT/PS/CI particles were compared with the pristine CI suspension through a rotational test under a variety of magnetic field strengths. The sedimentation of these particles was also examined.

* Corresponding author. Fax: +82 32 860 7486. E-mail: hjchoi@inha.ac.kr.
Received for review August 26, 2009 and accepted November 17, 2009
[†] Inha University.
[‡] Seoul National University.
DOI: 10.1021/am900577w

Published on Web 12/14/2009

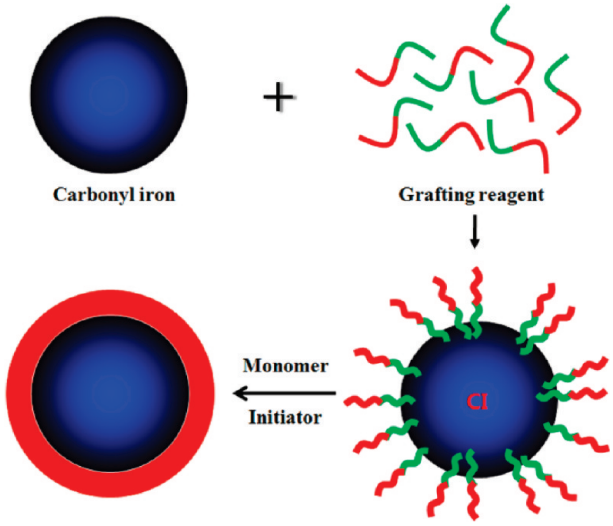

FIGURE 1. Schematic diagram of the synthesis of PS/CI composite particles.

2. EXPERIMENTAL SECTION

2.1. Synthesis of PS Nanobead-Coated CI Particles. At first, the PS nanobead-coated CI particles (CD grade, BASF, Ludwigshafen, Germany; average particle size = 4.25 μm, density = 7.91 g/cm^3) were synthesized using a conventional dispersion polymerization method (21). In order to improve the affinity between inorganic magnetic CI particles and the organic coating shell, 10 g of CI particles were modified with methacrylic acid (MAA; 99% purity, Junsei Chemical, Tokyo, Japan) by dispersion in a MAA (10 g)/methanol solution (100 g) under ultrasonification for 30 min. Subsequently, the CI/MAA/methanol dispersion was washed with additional methanol to remove the excess MAA. Then, the MAA-modified CI particles were mixed with 18 g of styrene monomer (99% purity, Samchun Chemical, Seoul, Korea) under agitation to prepare the polymerization of PS. The mixture was placed into a prepared methanol solution (200 g) containing 6.6 g of PVP (M_w = 1 300 000 g/mol, Junsei Chemical, Tokyo, Japan) as a stabilizer. The initiator, 0.54 g of 2,2′-azobis(isobutyronitrile) (Junsei Chemical, Tokyo, Japan), was then added into the reactor. Nitrogen (N_2) was purged during the reaction. The solution temperature was maintained at 55 °C for 24 h with vigorous stirring (rpm = 450). When the polymerization was complete, the final product was separated from the methanol solution of PVP or PS oligomers in excess using a magnet and dried at 60 °C for 24 h. A schematic diagram of the PS-coated CI particles steps is provided in Figure 1. The used grafting reagent (MAA) possesses two functional groups; the green part represents carboxylic acid, which is used to modify the surface of the CI particles, and the red part is considered to react with the vinyl radical of the styrene monomer, leading to successful polymerization of PS on the surface of the CI particles.

2.2. Fabrication of the MWCNT-Nest-Wrapped PS/CI Composite Particle. The MWCNT shells were produced using a simple solvent-casting methodology (23). First, the synthesized PS/CI particles were dispersed in a homogeneous dispersion of carboxylic acid functionalized MWCNT (24) in distilled water with vigorous stirring. This mixture was poured into a 100 mL silicone oil bath that had been preheated at 90 °C to form a W/O emulsion system. A considerably high stirring rate (rpm = 700) was used to evaporate as much water as possible at a relatively high temperature (90 °C). The suspension was cooled slowly to room temperature over a 6 h period and washed with excess acetone. The product obtained was dried in an oven for 24 h.

2.3. Sample Characterization Methods. The surface morphology of the pure CI particles, PS/CI particles, and MWCNT/PS/CI particles was observed by scanning electron microscopy (SEM; S-4200, Hitachi, Tokyo, Japan). The X-ray energy-dispersive spectroscopy (EDS) spectra were also obtained using an attached EDAX (coupled with a Hitachi S-4200) spectrometer. The section view of the PS/CI particles was studied by transmission electron microscopy (TEM; CM200, Philips, Mahwah, NJ). The sampling for TEM was carried out by dispersing the particles in an epoxy bath followed by nanoscaled cutting using an ultramicrotome and a final dropping onto a copper grid. The densities of the pure CI particles, PS/CI particles, and MWCNT/PS/CI particles were determined using a helium pycnometer (10 cm^3; AccuPyc 1130, Micromeritics, Norcross, GA). The determinations were carried out starting from the dried materials at room temperature. The magnetic measurements were carried out in the powder form at room temperature via a vibrating sample magnetometry (VSM; 7307, Lake Shore, Westerville, OH) with a maximum magnetic field of 650 kA/m.

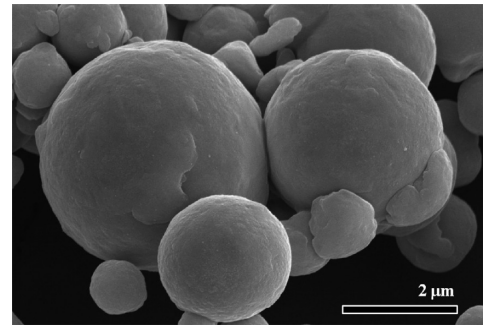

FIGURE 2. SEM image of the pure CI particles.

The fabricated MWCNT/PS/CI particles were dispersed in a lubricant oil (viscosity = 46.5 cSt; Yubase oil, SK Corp., Seoul, Korea) to prepare the MR fluid for MR characterization with a particle concentration of 20 vol %. In order to examine the influence of the coating process on the MR performance, a pure CI suspension was also prepared at the same volume percent. MR characterization of the two systems was performed using a rotational rheometer (Physica MC 300, Stuttgart, Germany) equipped with a magnetic field generator. All of the tests were performed at room temperature.

Finally, the sedimentation profile was recorded by taking snapshots for the pure CI suspension and MWCNT-wrapped PS/CI suspension as a function of time. In this method, the settling of the macroscopic phase boundary between the concentrated suspension and the supernatant liquid was observed. The sedimentation ratio is defined as (25)

$$\text{sedimentation ratio} = \frac{\text{volume of the supernatant liquid}}{\text{volume of the entire suspension}} \times 100$$

3. RESULTS AND DISCUSSION

3.1. Particles Morphology. Figure 2 shows the morphology of the pristine CI particles. The particles had a very smooth surface with a polydispersed size distribution.

After being treated with a MAA/methanol solution under ultrasonication, the morphology of the CI particles was preserved, as shown in Figure 3. Element analysis was performed by focusing the electron beam onto a single point of the surface of the MAA-modified CI particles to determine the composition of the surface. Figure 3 also shows the typical EDS spectra of the organic MAA-modified CI particles (the inset shows the chemical structure of MAA). Compared with the EDS data of pure CI particles (Figure S1 in the Supporting Information), which indicates an inorganic iron

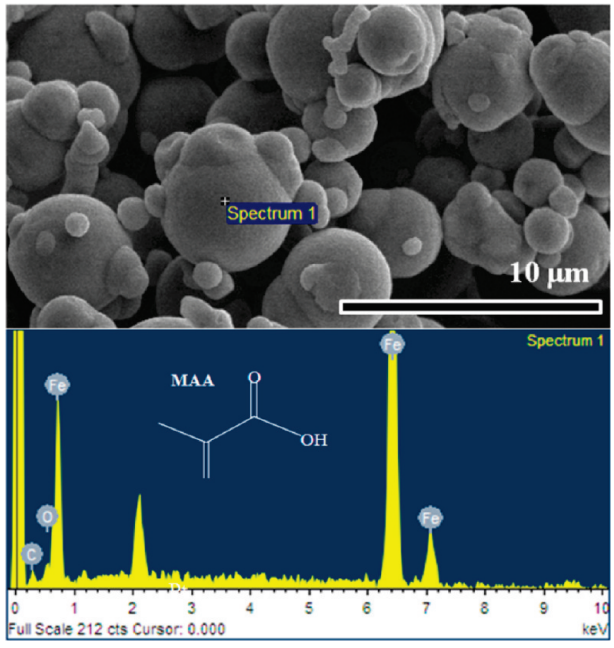

FIGURE 3. SEM image of MAA-modified CI particles (above) and EDS analysis (below).

Table 1. Element Composition of MAA-Modified CI Particles

element	weight %	atomic %
C	4.59	17.63
O	1.75	5.05
Fe	93.66	77.32

element, MAA-modified CI particles exhibit organic species (C and O) with strong intensity, as shown in Table 1. Therefore, modification with MAA does not affect the morphology of the CI particles but just introduces organic chemical functional groups to the CI particles.

The PS nanobeads were coated successfully onto the CI particles by using MAA as a grafting reagent, as shown in Figure 4a, in which many PS half-spheres with an almost monodispersed size distribution were spread over the surface of the MAA-treated CI particles. The free PS particles off the surface of the CI particles were also collected, and the morphology was observed, as shown in Figure 4b. The nanoscaled PS beads show a spherical shape with a very narrow particle size distribution. The average size of these PS nanobeads was approximately 250 nm, which coincides well with that of the semicircles on the surface of the CI particles.

The PS semibeads were nanosized mainly because of the high mechanical stirring rate (26). In this study, a high mechanical stirring rate was favored because of the high density of the CI particles, which may cause sedimentation defects during the reaction. Therefore, the stirring speed was increased to give a homogeneous suspension. The reason why these PS nano-half-spheres were synthesized on the surface of the CI particles rather than located randomly in the interspaces of the CI particles might be due to the MAA used. MAA was adopted in this experiment because it possesses a carboxyl functional group (hydrophilic) and a

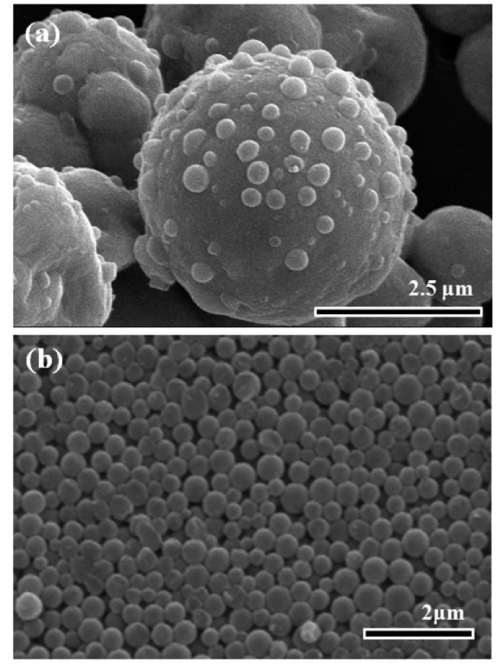

FIGURE 4. SEM images of (a) the PS-coated CI particles and (b) the free PS nanobeads.

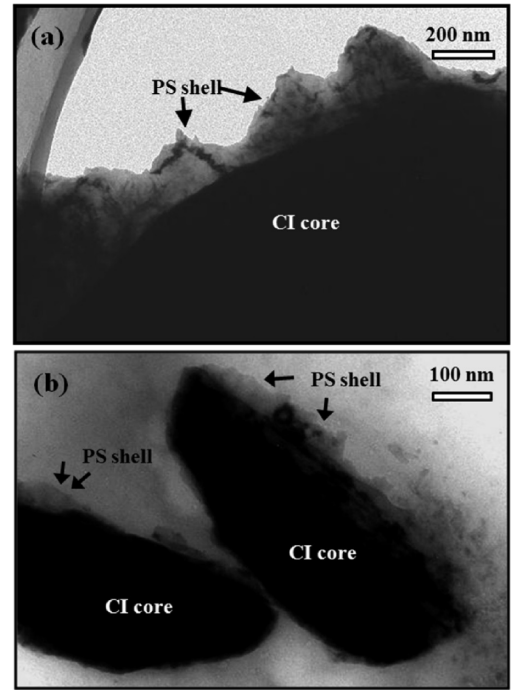

FIGURE 5. TEM images of the PS/CI particles with a semicircle (a) and a thin shell (b).

vinyl functional group (hydrophobic), giving it a good affinity to the CI particles and styrene monomer. In addition, the stabilizer, PVP, also plays a crucial role in the development of this structure (27).

Figure 5 shows the section view of the PS-coated CI particles. The light half-spheres represent the synthesized PS beads marked with the arrows, and the black cores indicate the CI particles. An apparent semicircular profile was observed along the surface of the CI particles. Two adjacent half-spheres either overlap or connect via a thin

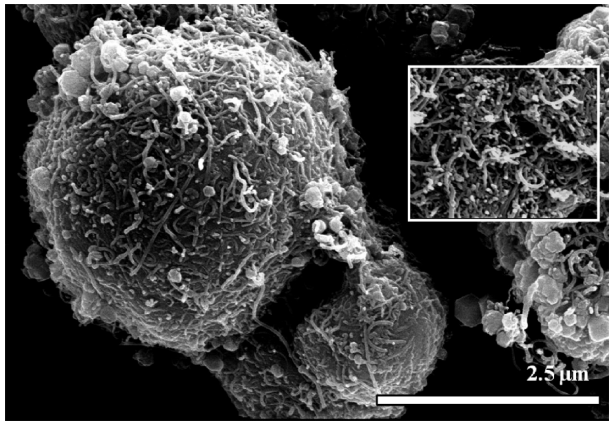

FIGURE 6. SEM image of MWCNT-wrapped PS/CI particles. The inset picture is an SEM image of the MWCNT used. The two photo shares the same scale bar.

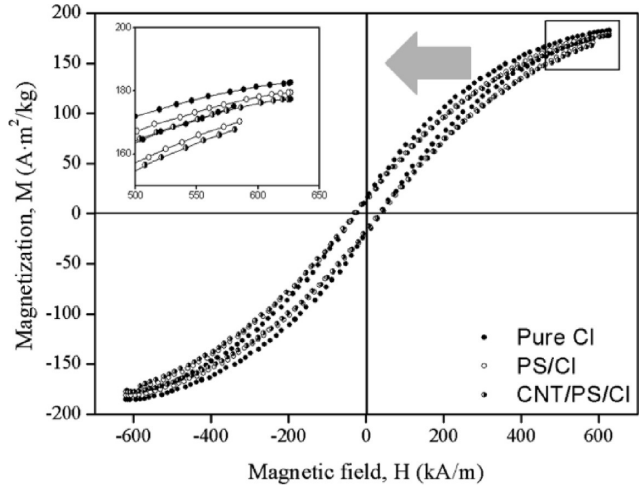

FIGURE 7. VSM data of the pure CI particles (closed symbol), PS/CI particles (open symbol), and MWCNT/PS/CI particles (semiclosed symbol). The inset is a magnified view of the saturation magnetization at high magnetic field strength.

layer. These half-spheres have dimensions similar to those determined from the SEM image. In some regions of the surface, where nanosized PS half-spheres are absent, a thin shell with a thickness of 40 nm can be seen clearly, as shown in Figure 5b. Therefore, both a thin PS shell and PS beads coat the surface of the CI particles. The sharp angles on the top of the half-spheres as well as the elongated CI core can be attributed to shape deformation occurring in the cutting process during TEM sample preparation.

Figure 6 shows the surface morphology of MWCNT-wrapped PS/CI particles. The inset is the acid-treated MWCNT, whose mean diameter is approximately 15 nm. Many MWCNTs were piled together, forming a dense MWCNT network over the entire surface of the PS/CI particles. Some considerably tiny PS beads were covered completely by the MWCNT nests and were invisible. The surface of the MWCNT/PS/CI particles was quite rough compared to that of the pure CI or PS/CI particles. When this simple W/O emulsion methodology was adopted, well-dispersed MWCNTs tended to aggregate by self-assembly around the surface of the PS/CI particles, forming a dense nest when water was evaporated at high temperatures. The driving force was assumed to be nanotube−nanotube interactions and hydrogen bonding from the carboxyl and hydroxyl groups. This method has been used to fabricate novel MWCNT capsules (22), and recently polymer colloids with an interfacial coating of purified single-walled carbon nanotubes were also synthesized (28).

Considering the above-mentioned observation, the mechanism for the formation of MWCNT/PS/CI particles was proposed. To improve the sedimentation problem, organic PS was first synthesized on the surface of the CI particles using a grafting reagent. Instead of a conventional perfect core−shell structure, a very thin PS shell with many PS nano-half-spheres over the surface of the CI particles was observed, which was attributed to the vigorous stirring used to prevent the settling of the CI particles. Although the synthesized PS/CI composite particles showed a lower density, they also exhibited a smooth surface similar to that of pure CI particles. Therefore, a second-stage wrapping of a MWCNT nest was constructed on the surface of the PS shell to produce a rough surface, which would improve the sedimentation stability.

3.2. Magnetic Properties. Figure 7 shows the magnetic hysteresis loops of the pure CI particles, synthesized PS/CI particles, and MWCNT/PS/CI particles measured in the powder state. The three curves show similar saturation magnetization. In a magnified view (the inset graph), the saturation magnetization values for the pure CI, PS/CI, and MWCNT/PS/CI particles were 182.58, 179.48, and 177.52 $A \cdot m^2/kg$, respectively. This slight difference in the saturation magnetization was attributed to the introduction of organic PS half-spheres and deposited MWCNT nests. Therefore, the MR suspension based on the MWCNT/PS/CI powder may have weaker MR performance than the pure CI particles because the saturation magnetization is a crucial factor for the superior MR effect. However, the intrinsic hysteresis behavior of the CI particles was maintained in both the PS/CI and MWCNT/PS/CI particles.

3.3. MR Behavior. MR characterization was performed using a rotational rheometer in controlled shear rate (CSR) mode and controlled shear stress (CSS) mode. For a typical CSR test, the shear rates tested ranged from 0.01 to 200 s^{-1} on a log−log scale. Shearing MR fluids with a too high shear rate might cause their expulsion during the measurement between the disks with a parallel-plate geometry. For each shear rate sweep, the duration of the measuring point was set from an initial 10 s to a final 1 s on a log−log scale. The resulting flow responses were examined as a function of the magnetic field strength ranging from 0 to 343 kA/m, as indicated in Figure 8 (29, 30). A MR fluid based on pure CI particles was also prepared at the same volume concentration (20 vol %) to compare the influence of the wrapped MWCNT/PS shell on the MR behavior, as marked by the lines in Figure 8. Both suspensions indicate a wide plateau region through the whole shear rate range (31). As expected, the shear stress obtained has a strong dependence on the applied field strength, which is similar to the phenomenon observed for ER fluids (32, 33). This

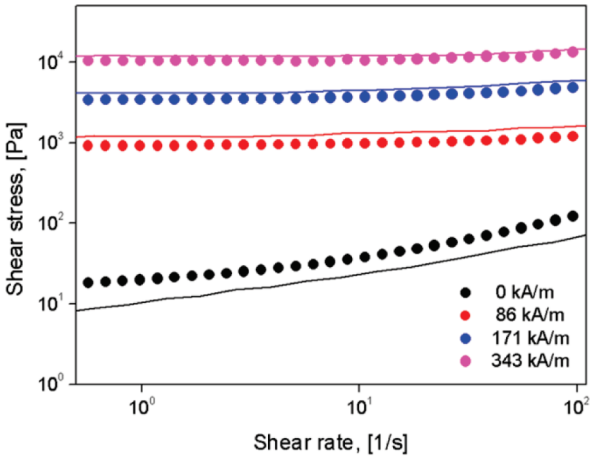

FIGURE 8. Rheogram obtained via CSR mode for 20 vol % of the MWCNT/PS/CI suspension (points) and pure CI suspension (lines) under different magnetic field strengths.

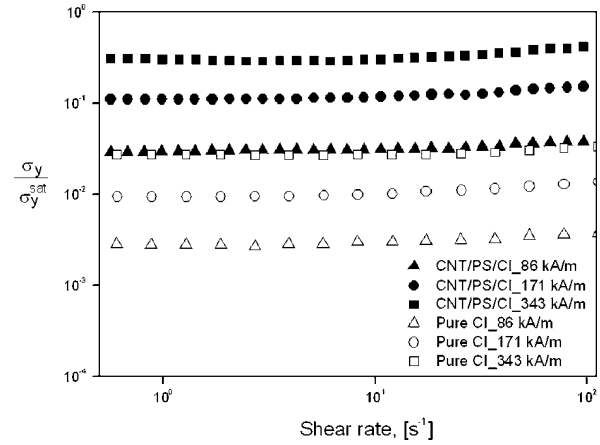

FIGURE 9. Normalized rheogram of the MWCNT/PS/CI suspension (closed symbol) and pure CI suspension (open symbol) under different magnetic field strengths.

observation was attributed to the robust columns formed because of the strong dipole−dipole interactions between adjacent magnetic particles.

Compared to the shear stress value without a magnetic field, the MWCNT/PS/CI suspension exhibited a much higher shear stress than the pure CI suspension. In addition, unlike the curve of the pure CI suspension, which shows a straight line, the curve of the MWCNT/PS/CI suspension appeared to have a nonzero yield stress at an almost zero shear rate. This observation was predicted by analyzing the unique morphology of the MWCNT/PS/CI particles. After wrapping them via two separate steps, the densely piled MWCNT nest composed of many MWCNTs over the surface of the PS-coated CI particles produced a considerably rough surface compared to the relatively smooth surface of the pure CI particles. When an external shear field was exerted, these rough particles had sufficient opportunity to come in contact with each other, and the adsorbed MWCNTs caused flocculation by bridging the gap between the adjacent CI particles (34). These MWCNTs are believed to resemble those cross-linkers that bind the ambient MWCNT/PS/CI particles together. Evidently, this bridging-flocculated MWCNT/PS/CI suspension suggests enhanced rheological behavior (apparent viscosity, yield stress, and modulus) compared to the pure CI suspension.

When a magnetic field is present, the shear stress of the MWCNT/PS/CI suspension indicates a lower value than that of the pure CI suspension under the same magnetic field strength. The flocculation induced by the rough surface does not appear to enhance the shear stress as it does without a magnetic field. In a recently reported MR system composed of cobalt fibers, another term, solid friction, combined with the field-induced magnetic attraction was believed to promote the increased shear stress (35−37). In the case of a cobalt fiber suspension, upon application of a magnetic field, the alignment of the fibers along the direction of the field was hindered by friction within the fiber-entangled network, which was formed by three types of contact: side-by-side, side-by-end, and end-by-end (less frequent). Therefore, enhanced shear stress was achievable. In this system, the rough surface causes flocculation or friction, which might increase the shear stress as it does without a magnetic field. However, compared to the bulk magnetic properties of the cobalt fiber network, these MWCNT/PS/CI particles have a magnetic CI core, a nonmagnetic middle PS shell, and weak magnetic MWCNT nests. Introducing a polymeric shell will inevitably have an adverse effect on the saturation magnetization, as shown in the VSM data, which can lead to decreased rheological properties (shear stress, shear viscosity, and modulus). The second step, wrapping with a MWCNT nest, was used to cause flocculation or friction in order to compensate for the decreased shear stress. Unfortunately, there was little difference in shear stress between the pure CI suspension and the MWCNT/PS/CI suspension, as shown in Figure 7. Nevertheless, this difference was relatively small compared to other polymer-coating systems. In addition, the coated PS beads (~200 nm) rather than the PS shell play some negative role in the rheological behavior. Therefore, the thickness and morphology of the polymer shell along with the MWCNT nest should be adjusted carefully to obtain enhanced rheological properties.

In order to determine if this coating process induces solid friction between the particles, the rheogram in Figure 9 was replotted by scaling the shear stress by the square of the saturation magnetization of particles, as shown in Figure 8. At very high magnetic field strengths, the magnetization saturates throughout the particles, and the yield stress becomes independent of the applied field (38):

$$\sigma_y^{sat} = 0.086\phi\mu_0 M_s^2 \quad (1)$$

where φ is the volume concentration of the MR suspension (20 vol %), $\mu_0 = 4\pi \times 10^{-7}$ Tm/A is the permeability of free space, and M_s is the saturation magnetization, which can be estimated from Figure 7 for both MWCNT/PS/CI and pure CI particles. The estimated yield stresses for the MWCNT/PS/CI and pure CI particles at the saturation region were 31.67 and 43.97 kPa, respectively. In Figure 9, the MWCNT/PS/CI suspension indicates higher normalized shear stress than that of the pure CI suspension, suggesting that the shear stress was enhanced by flocculation from the solid friction induced by two-step wrapping.

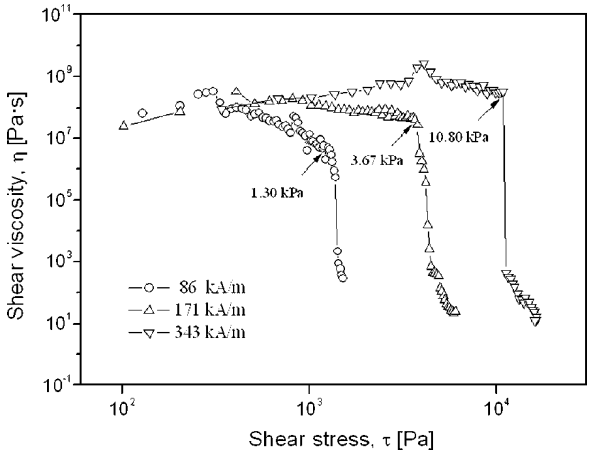

FIGURE 10. Rheogram obtained via the CSS mode for 20 vol % of the MWCNT/PS/CI suspension under different magnetic field strengths.

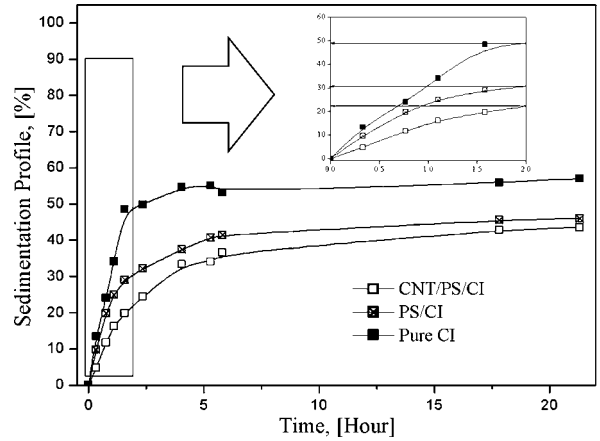

FIGURE 11. Sedimentation profile recorded as a function of time for pure CI, PS/CI, and MWCNT/PS/CI suspensions. The inset figure is a magnified view of the sedimentation ratio tested at an initial 2 h.

Compared to the above dynamic yield stress, the static yield stress was also examined using the CSS approach, which starts testing in the rest state and increases the stress to a critical value at which the sample begins to flow (39). Figure 10 shows the change in the viscosity as a function of the shear stress, in which the shear viscosity initially holds its value at the low shear rate region and then falls abruptly, finally approaching a constant value at high shear stress. The static yield stress develops below a value in which there is no real macroscopic flow. From the point marked with the arrowhead, all of the curves show a fairly sharp decrease in the shear viscosity. Therefore, the value of this point can be considered to be the static yield stress, which is approximately 1.30, 3.67, and 10.80 kPa corresponding to 86, 171, and 343 kA/m, respectively. Indeed, the sample undergoes creep behavior below this stress, but it is assumed to be static.

3.4. Sedimentation Characterization. The sedimentation observation of pure CI, PS/CI, and MWCNT/PS/CI suspensions was examined. The densities of the pure CI particles, PS/CI particles, and MWCNT/PS/CI particles were 7.91, 7.41, and 6.82 g/cm^3, respectively. This tiny decrease in the density, which coincides with the VSM data, apparently causes a decrease in the density mismatch with the oil (density = 0.84 g/cm^3), consequently leading to an expected improvement in the sedimentation ratio (14, 20, 21, and 340). Figure 11 shows the recorded sedimentation profile as a function of time, in which the pure CI suspension exhibits the highest sedimentation ratio, suggesting that the supernatant layer of the pure CI suspension is longer than the other two suspensions, which, consequently, means that pure CI particles settle rapidly and seriously during the same time duration. In contrast, the MWCNT/PS/CI suspension indicates the lowest value of the sedimentation ratio. Thus, the lower the sedimentation ratio is, the better is the dispersion stability. This improved sedimentation observation was attributed to the apparently reduced mismatch in the density, which has been found to be quite effective in many polymer-coating systems. In addition, the flocculation due to the considerably rough surface may form a network that retards sedimentation.

Indeed, a homogeneous redispersion of the MWCNT/PS/CI suspension could be obtained easily by momentary mild shaking after completing the MR test and allowing sufficient time for all of the particles to settle. Therefore, the improved dispersion stability and the easy redispersion can be attributed to the reduced density and rough surface.

4. CONCLUSIONS

Both conventional dispersion polymerization and an easy W/O system were used to fabricate novel MWCNT/PS/CI particles to improve the dispersion stability of MR fluids. A successful coating of PS nano-half-spheres along with the subsequent dense MWCNT nests on the surface of the CI particles was confirmed from the SEM/TEM images. The decreased saturation magnetization shown in the VSM data corresponds well to the decreased density. The MWCNT-coated PS/CI particles indicate a little decreased MR performance under magnetic field due to the weaker saturation magnetization but enhanced shear behavior without magentic field owing to the induced flocculation from the fairly rough surface. Finally, a MWNT-coated PS/CI suspension exhibits better dispersion stability as well as redispersionality.

Acknowledgment. The authors acknowledge Hwang Sun Jae for valuable assistance with the TEM. This study was supported by KOSEF (Grant R01-2006-000-10062-0).

Supporting Information Available: EDX spectra of pure CI particles. This material is available free of charge via the Internet at http://pubs.acs.org.

REFERENCES AND NOTES

(1) Bombard, A. J. F.; Knobel, M.; Akantara, M. R. *Int. J. Mod. Phys. B* **2007**, *21*, 4858–4867.
(2) Bica, I.; Choi, H. J. *Int. J. Mod. Phys. B* **2008**, *22*, 5041–5064.
(3) See, H.; Joung, C.; Ekwebelam, C. *Int. J. Mod. Phys. B* **2007**, *21*, 4945–4951.
(4) Guerrero-Sanchez, C.; Lara-Ceniceros, T.; Jimenez-Regalado, E.; Rasa, M.; Schubert, U. S. *Adv. Mater.* **2007**, *19*, 1740–1747.

(5) Pu, H. T.; Jiang, F. J.; Yang, Z. L. *Mater. Lett.* **2006**, *60*, 94–97.
(6) Viota, J. L.; de Vicente, J.; Duran, J. D. G.; Delgado, A. V. *J. Colloid Interface Sci.* **2005**, *284*, 527–541.
(7) Bica, I. *J. Ind. Eng. Chem.* **2007**, *13*, 693–711.
(8) (a) López-López, M. T.; Gomez-Ramirez, A.; Durán, J. D. G.; González-Caballero, F. *Langmuir* **2008**, *24*, 7076–7084. (b) Cho, E. C.; Shim, J.; Lee, K. E.; Kim, J. W.; Han, S. S. *ACS Appl. Mater. Interfaces* **2009**, *1*, 1159–1162.
(9) Choi, H. J.; Jhon, M. S. *Soft Matter* **2009**, *5*, 1562–1567.
(10) Wen, W. J.; Huang, X. X.; Sheng, P. *Soft Matter* **2008**, *4*, 200–210.
(11) Cho, M. S.; Cho, Y. H.; Choi, H. J.; Jhon, M. S. *Langmuir* **2003**, *19*, 5875–5881.
(12) Kamath, G. M.; Hurt, M. K.; Werely, N. M. *Smart Mater. Struct.* **1996**, *5*, 576–590.
(13) Goncalves, F. D.; Carlson, J. D. *Int. J. Mod. Phys. B* **2007**, *21*, 4832–4840.
(14) Jang, I. B.; Kim, H. B.; Lee, J. Y.; You, J. L.; Choi, H. J.; Jhon, M. S. *J. Appl. Phys.* **2005**, *97*, in press.
(15) de Vicente, J.; López-López, M. T.; Durán, J. D. G.; González-Caballero, F. *Rheol. Acta* **2004**, *44*, 94–103.
(16) Tang, X.; Zhang, X.; Tao, R.; Rong, Y. *J. Appl. Phys.* **2000**, *87*, 2634–2638.
(17) de Vicente, J.; López-López, M. T.; González-Caballero, F.; Durán, J. D. G. *J. Rheol.* **2003**, *47*, 1093–1099.
(18) Lim, S. T.; Choi, H. J.; Jhon, M. S. *IEEE Trans. Magn.* **2005**, *41*, 3745–3747.
(19) Fang, F. F.; Jang, I. B.; Choi, H. J. *Diamond Relat. Mater.* **2007**, *16*, 1167–1169.
(20) Cho, M. S.; Lim, S. T.; Jang, I. B.; Choi, H. J.; Jhon, M. S. *IEEE Trans. Magn.* **2004**, *40*, 3036–3038.
(21) Fang, F. F.; Choi, H. J. *Phys. Status Solidi A* **2007**, *204*, 4190–4193.
(22) Pu, H. T.; Jiang, F. J.; Yang, Z. L.; Yan, B. *J. Appl. Polym. Sci.* **2006**, *102*, 1653–1657.
(23) Yi, H.; Song, H.; Chen, X. *Langmuir* **2007**, *23*, 3199–3204.
(24) Park, S. J.; Cho, M. S.; Lim, S. T.; Choi, H. J.; Jhon, M. S. *Macromol. Rapid Commun.* **2003**, *24*, 1070–1073.
(25) Park, J. H.; Kwon, M. H.; Park, O. O. *Korean J. Chem. Eng.* **2001**, *18*, 580–585.
(26) Arshady, R. *Colloid Polym. Sci.* **1992**, *270*, 717–732.
(27) Guo, L.; Pei, G.; Wang, T.; Wang, Z.; Jin, Y. *Colloids Surf. A* **2007**, *293*, 58–62.
(28) Hobbie, E. K.; Fagan, J. A.; Obrzut, J.; Hudson, S. D. *ACS Appl. Mater. Interfaces* **2009**, *1*, 1561–1566.
(29) Wereley, N. M.; Chaudhuri, A. J.; Yoo, H.; John, S.; Kotha, S.; Suggs, A.; Radhakrishnan, R.; Love, B.; Sudarshan, J. T. S. *J. Intell. Mater. Syst. Struct.* **2006**, *17*, 393–401.
(30) Rankin, P. J.; Horvath, A. T.; Klingenberg, D. J. *Rheol. Acta* **1999**, *38*, 471–477.
(31) Ekwebelam, C.; See, H. *Rheol. Acta* **2009**, *48*, 19–32.
(32) Cho, Y. H.; Cho, M. S.; Choi, H. J.; Jhon, M. S. *Colloid Polym. Sci.* **2002**, *280*, 1062–1065.
(33) Sung, J. H.; Jang, W. H.; Choi, H. J.; Jhon, M. S. *Polymer* **2005**, *46*, 12359–12365.
(34) Larson, R. G. Particle gels. In *The Structure and Rheology of Complex Fluids*; Gubbins, K. E., Barteau, M. A., Cussler, E. L., Jensen, K. F., Lauffenburger, D. A., Morari, M., Harmon Ray, W.; Russel, W. B., Eds.; Oxford University Press Inc.: New York, 1999; pp 324—357.
(35) Switzer, L. H.; Klingenberg, D. J. *Int. J. Multiphase Flow* **2004**, *30*, 67–87.
(36) López-López, M. T.; Kuzhir, P.; Bossis, G. *J. Rheol.* **2008**, *53*, 115–126.
(37) Kuzhir, P.; López-López, M. T.; Bossis, G. *J. Rheol.* **2008**, *53*, 127–151.
(38) (a) Ginder, J. M.; Davis, L. C.; Elie, L. D. *Int. J. Mod. Phys. B* **1996**, *10*, 3293–303. (b) Fang, F. F.; Choi, H. J.; Jhon, M. S. *Colloids Surf. A* **2009**, *351*, 46–51.
(39) Uhlherr, P. H. T.; Guo, J.; Fang, T. N.; Tiu, C. *Korea—Aust. Rheol. J.* **2002**, *14*, 17–23.
(40) Lee, M. A.; Fang, F. F.; Choi, H. J. *Phys. Status Solidi A* **2007**, *204*, 4186–4189.

AM900577W